Chalcogenide Letters Vol. 12, No. 10, October 2015, p. 529 - 536

INFLUENCES OF LOW TEMPERATURE POST-ANNEALING ON THE SULFURIZED Cu_2ZnSnS_4 THIN FILMS

J. X. XU*, Z. M. CAO, Y. Z. YANG
School of Materials and Energy, Guangdong University of Technology, Guangzhou 510006, China

In this work, after the sulfurization of Cu-Zn-Sn precursors, the sulfurized thin films were post annealed to further enhance the properties of Cu_2ZnSnS_4 thin films. The post-annealing was performed at low temperature in a sulfur-free atmosphere to avoid the decomposition of Cu_2ZnSnS_4. The effect of annealing temperature was studied by XRD, Raman, SEM, and UV-vis spectrophotometer measurements. The experimental results demonstrate that the structural properties of Cu_2ZnSnS_4 thin films enhance after annealing at 250 and 300 ^oC as the grains of thin films enlarge with increasing annealing temperature. However, when the annealing temperature increases to 350 ^oC, the grain size and compactness of thin films reduce. Besides, the appearance of secondary phase of Cu_2SnS_3 indicates the decomposition of Cu_2ZnSnS_4. Therefore, post annealing at appropriate temperature is a useful way to improve the properties of Cu_2ZnSnS_4 thin films. A low temperature of post annealing should be chosen to avoid the decomposition of Cu_2ZnSnS_4.

(Received September 9, 2015; Accepted October 23, 2015)

Keywords: Cu_2ZnSnS_4; Annealing; Decomposition; Structural properties

1. Introduction

In recent years, the earth-abundant Cu_2ZnSnS_4 (CZTS) has been proposed as promising absorber material for thin film solar cell applications [1-4]. The structural, electrical, and optical properties of Cu_2ZnSnS_4 thin films are similar with those of current $Cu(In,Ga)Se_2$ thin films [5-6]. The advantages of Cu_2ZnSnS_4 are that its constituent elements are non-toxic, abundance, and low-cost. The solar cell can be made by substituting Cu_2ZnSnS_4 absorber into a standard $Cu(In,Ga)Se_2$ solar cell [7-9]. The conversion efficiency record of Cu_2ZnSnS_4-based thin film solar cell has been achieved 12.6% in 2013 [10].

The quality of Cu_2ZnSnS_4 absorber plays an essential role on the photovoltaic performances of solar cell. The studies of Cu_2ZnSnS_4 solar cell focus on the fabrication and characterization of absorber [11-13]. The Cu_2ZnSnS_4 absorber needs single-phase, large grain size, reduced defects, large absorption coefficient, and suitable band gap for solar cell application. In our previous studies, we have used magnetron sputtering and post-sulfurization methods to prepare single-phase Cu_2ZnSnS_4 thin films [14,15]. The measured results show that the prepared Cu_2ZnSnS_4 thin films are suitable as absorber. However, the properties of Cu_2ZnSnS_4 thin films are still needed to be further enhanced.

Heat treatment is a useful way to improve the characteristics of materials. In previous works, we have proved that annealing can effectively enhance the crystallinity of sputtered SnS

*Corresponding author xujiaxiong@gdut.edu.cn

thin films [16]. However, for Cu_2ZnSnS_4, after the formation of Cu_2ZnSnS_4 phase, the Cu_2ZnSnS_4 decomposes easily in the sulfur atmosphere [17-19]. Increasing sulfurization temperature or time of Cu_2ZnSnS_4 may lead to the formation of secondary phases, which is unfavorable for the properties of Cu_2ZnSnS_4. In present work, we tried to perform post-annealing in a sulfur-free atmosphere for the Cu_2ZnSnS_4 thin films fabricated by sulfurization of sputtered Zn/Sn/Cu precursors. The sulfurized thin films were annealed at low temperature to try to avoid the decomposition of Cu_2ZnSnS_4. The structural, morphological, and optical properties of prepared thin films were measured to study the effects of post-annealing treatment.

2. Experimental method

The fabrications of Cu_2ZnSnS_4 thin films were composed of three steps of sputtering, sulfurization, and post-annealing. Before the deposition of thin films, the soda-lime glass substrates were cleaned sequentially in acetone, absolute ethyl alcohol, and deionized water by ultrasonic cleaning method. After dried by nitrogen flow, the substrates were transferred into a magnetron sputtering system (FJL560). The chamber of magnetron sputtering system was evacuated to a base pressure of 5×10^{-4} Pa. Then, the pure argon with a flow of 20 ml/min was introduced into the chamber. The working pressure was maintained at 0.5 Pa during sputtering. The Mo thin films were first sputtered on the soda-lime glass substrates. After the deposition of Mo, the metal Zn, Sn, and Cu were sputtered sequentially to form Zn/Sn/Cu stacked precursors. Detailed sputtering process had been described in our previous works [14,15].

The sputtered Zn/Sn/Cu stacked precursors were then sulfurized in a tubular furnace. The sulfurization atmosphere was $S+N_2$. The sulfur vapor was produced by the evaporation of sulfur powders. Fig. 1 shows the change of furnace temperature with time. The target sulfurization temperature was 500 ^oC. At this temperature, the sulfurization time was 20 min.

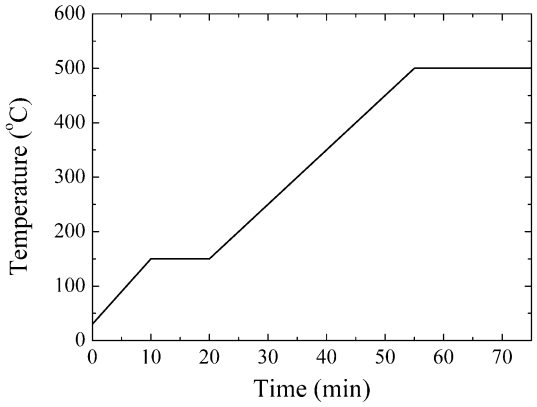

Fig. 1 Schematic of the temperature change in the sulfurization treatment

After the sulfurization treatment, post-annealing was carried out in a sulfur-free atmosphere. Three low annealing temperatures of 250, 300, and 350 ^oC were chosen. The annealing time was fixed at 30 min. During annealing, the pure nitrogen flow was introduced into the furnace as protective gas. After annealing, the samples naturally cooled down in the nitrogen atmosphere.

The crystalline structures of prepared thin films were measured by X-ray diffractometry (XRD, Rigaku D/MAX-Ultima IV, Cu-kα radiation) and Raman spectroscopy (HORIBA Jobin Yvon, LabRAM HR800, λ=633 nm). The scanning electron microscopy (SEM, Hitachi S3400N) was used to observe the surface and cross section morphologies of Cu_2ZnSnS_4 thin films. The optical properties of prepared thin films were measured by UV-vis spectrophotometer (Pgeneral, T6). For the measurements of optical properties, we also prepared annealed Cu_2ZnSnS_4 thin films without Mo layer.

3. Results and discussion

3.1 The structural properties of Cu_2ZnSnS_4 thin films

The structural properties of Cu_2ZnSnS_4 thin films without annealing and with different annealing temperatures were first characterized by XRD and the results are shown in Fig. 2. In Fig. 2, the XRD peaks located at 18.3°, 28.5°, 33.0°, 47.4°, and 56.2° are attributed to the (101), (112), (200), (220), and (312) planes of kesterite Cu_2ZnSnS_4, respectively. The preferred orientation is along the (112) plane, which is consisting with other reports and our previous works [14,15,20-24]. The XRD peaks of secondary phases of Cu_xS and Sn_xS are absent in Fig. 2. In addition, the XRD peaks at 40.5° come from the Mo layer.

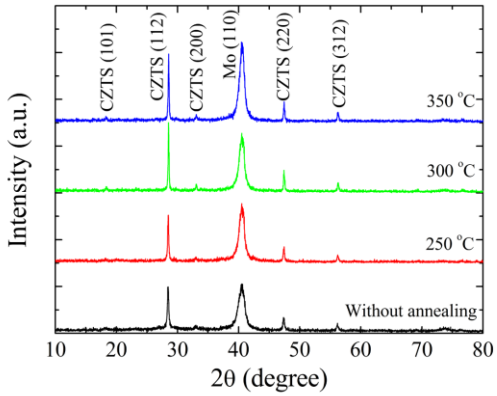

Fig. 2 The XRD patterns of prepared thin films without annealing and with different annealing temperatures

We further study the effect of annealing temperature on the structural properties of Cu_2ZnSnS_4 thin films. Table 1 lists the full width at half maximum (FWHM) of the (112) peak, grain size, and dislocation density of Cu_2ZnSnS_4 thin films with the change of annealing condition. The grain sizes are calculated by Debye–Scherrer equation. The dislocation densities (δ) are calculated by

$$\delta = \frac{1}{D^2}$$

where D is the grain size of thin films. As seen in Table 1, the calculated grain sizes of annealed

thin films are larger than that of thin film without annealing, indicating that post-annealing treatment can improve the structural properties of Cu_2ZnSnS_4 thin films. For annealing temperature no more than 300 ^oC, the crystallinity of Cu_2ZnSnS_4 thin films enhances with increasing annealing temperature. The thin films annealed at 300 ^oC show the maximum grain size and the minimum dislocation density. However, when the annealing temperature increases to 350 ^oC, the value of FWHM increases, resulting in reduced grain size and increase dislocation density. Therefore, the crystallinity of Cu_2ZnSnS_4 thin films annealed at 350 ^oC is lower than that of thin films annealed at 300 ^oC.

Table 1 The full width at half maximum (FWHM) of the (112) peak, grain size, and dislocation density of thin films with annealing temperature.

Annealing temperature (^oC)	FWHM (^{o})	Grain size (nm)	Dislocation density (10^{-4} nm^{-2})
Without annealing	0.277	43.0	5.41
250	0.203	58.6	2.91
300	0.162	73.5	1.85
350	0.171	69.7	2.06

The structural properties of prepared thin films were also measured by Raman spectroscopy to characterize the phase structures more exactly. Fig. 3 shows the Raman spectra of all prepared thin films. The Raman peaks at 265, 288, 338, and 367 cm^{-1} are assigned to the quaternary Cu_2ZnSnS_4 phase. For all samples, the strongest Raman peaks located at 338 cm^{-1} are original from the A_1 mode of Cu_2ZnSnS_4, which agree with the reported results [21,23-25]. However, the Raman peak at 321 cm^{-1} comes from the secondary phase of Cu_2SnS_3. The results of Raman measurements reveal that the thin films without annealing and with annealing temperatures of 250 and 300 ^oC are single-phase Cu_2ZnSnS_4. The Raman peaks of Cu_2ZnSnS_4 are the highest when the annealing temperature is 300 ^oC, indicating the enhancement in the structural properties of thin films after annealing. When the annealing temperature increases to 350 ^oC, the reduced Cu_2ZnSnS_4 peak intensity at 338 cm^{-1} and the present Cu_2SnS_3 peak mean the decomposition of Cu_2ZnSnS_4 phase.

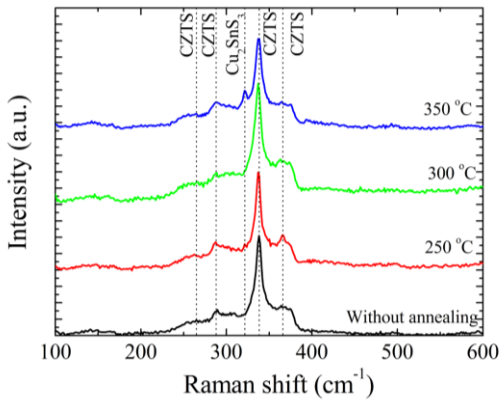

Fig. 3 The Raman scattering spectra of prepared thin films without annealing and with different annealing temperatures

The results of XRD and Raman measurements demonstrate that post-annealing at 250 and 300 ^{o}C can improve the structural properties of sulfurized Cu_2ZnSnS_4 thin films. The post-annealing treatment can provide energies to the further growth of Cu_2ZnSnS_4 structure. So the grain size of Cu_2ZnSnS_4 increases after post-annealing. The grain size of Cu_2ZnSnS_4 thin films annealed at 300 ^{o}C is larger than that of thin films annealed at 250 ^{o}C. However, for the annealing temperature of 350 ^{o}C, the instability of Cu_2ZnSnS_4 leads to the decomposition of Cu_2ZnSnS_4, which is adverse for the Cu_2ZnSnS_4 thin films. Therefore, the sulfurized Cu_2ZnSnS_4 thin films should be post annealed at low temperature.

3.2 The morphological properties of Cu_2ZnSnS_4 thin films

Fig. 4 shows the SEM images of the surfaces of prepared thin films. As revealed from the SEM images, all samples show grainy morphologies in the surface and the grains are near circular. For the thin films without annealing, the thin film surface is compact, uniform, and smooth. Besides, the grains aggregate in some regions. After post-annealing at 250 ^{o}C, the grains enlarge slightly. For the thin films annealed at 300 ^{o}C, the grain size of thin films increases significantly and the grainy morphology is more distinct. However, when the annealing temperature increases to 350 ^{o}C, the grain size of thin films reduces as compared with that of thin films annealed at 300 ^{o}C. The compactness of thin films reduces as some voids appear in the surface.

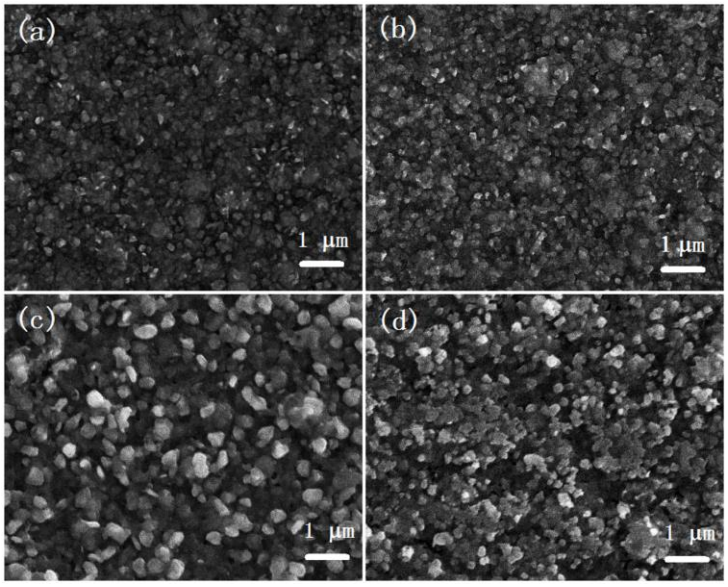

Fig. 4 The surface SEM images of Cu_2ZnSnS_4 thin films (a) without annealing and after post-annealing at (b) 250 ℃, (c) 300 ℃ and (d) 350 ℃

Fig. 5 shows the cross-sectional SEM images of Cu_2ZnSnS_4 thin films. The cross-sectional images indicate that the thin films become more compact for annealing temperature increases to 300 ^{o}C. The thin films annealed at 350 ^{o}C are less compact, which is consisting with the surface images in Fig. 4. From Fig. 5, the thicknesses of all thin films are obtained as about 1 μm. The results of SEM measurements in Fig. 4 and Fig. 5 are in agreements with the XRD and Raman results.

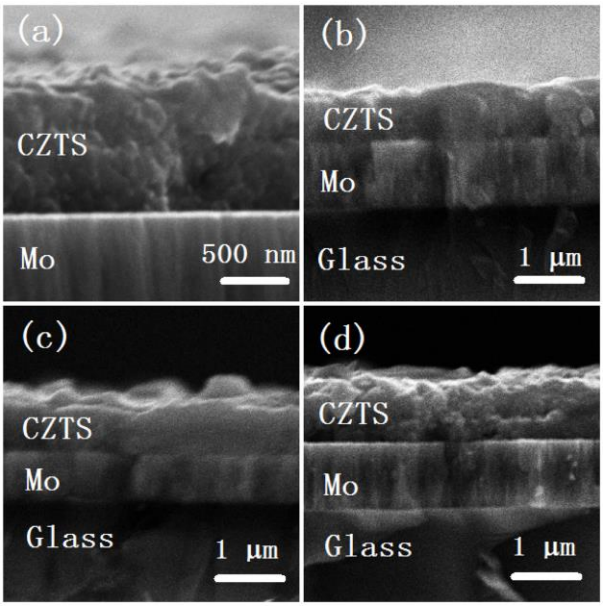

Fig. 5 The cross-sectional SEM images of Cu_2ZnSnS_4 thin films (a) without annealing and after post-annealing at (b) 250 ℃, (c) 300 ℃ and (d) 350 ℃.

3.3 The optical properties of Cu_2ZnSnS_4 thin films

The transmittances of Cu_2ZnSnS_4 thin films in the visible light and near infrared regions are shown in Fig. 6. The transmittances of all samples reduce with decreasing wavelength because of the absorption of incident photons. From the transmittance spectra, we can obtain the absorption coefficients (α) of Cu_2ZnSnS_4 thin films by

$$\alpha = \frac{1}{d} \ln \frac{1}{T}$$

where T and d are the transmittance and thickness of thin films, respectively.

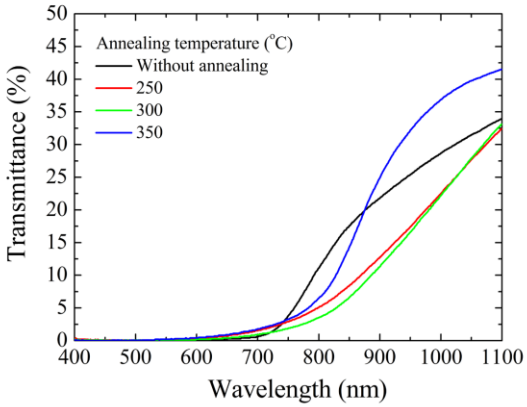

Fig. 6 The transmittance spectra of all Cu_2ZnSnS_4 thin films

We can further obtain the optical band gap of prepared thin films from the $(\alpha h\nu)^2$-$h\nu$ curves in Fig. 7. The relation between $(\alpha h\nu)^2$ and $h\nu$ can be described as

$$(\alpha h\nu)^2 = A(h\nu - E_g)$$

where $h\nu$ is the photon energy, E_g is the direct optical band gap of material, and A is a constant. In Fig. 7, all $(\alpha h\nu)^2$-$h\nu$ curves show linear properties in the high energy region. By extrapolating the linear region of curves to the $h\nu$ axis, the intercept of $h\nu$ axis gives the direct optical band gap. The direct optical band gap of Cu_2ZnSnS_4 thin films without annealing is 1.61 eV. For the annealed thin films, their direct optical band gaps are 1.51, 1.48, and 1.48 eV when the annealing temperatures are 250, 300, and 350 °C, respectively. The direct optical band gaps of annealed thin films are close to the reported results, which is suitable for absorber [20,21,24,25]. The reduced optical band gaps of annealed thin films result from the quantum confinement effect.

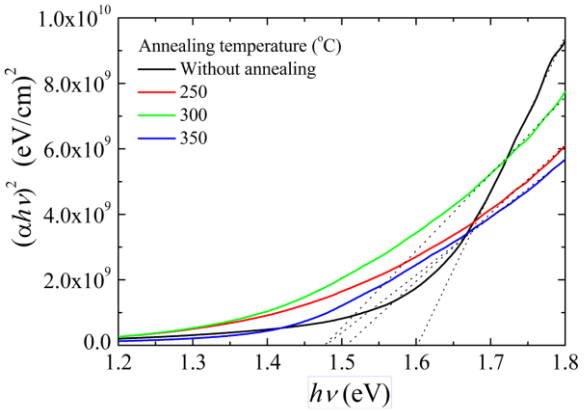

Fig. 7 The $(\alpha h\nu)^2$–$h\nu$ curves of all Cu_2ZnSnS_4 thin films.

4. Conclusion

The Cu_2ZnSnS_4 thin films were sequentially fabricated by sputtering of precursors, sulfurization, and post-annealing. The properties of prepared thin films were characterized to study the influences of post-annealing. For thin films without annealing and with annealing temperatures of 250 and 300 °C, the thin films are single-phase Cu_2ZnSnS_4 and the crystallinity of Cu_2ZnSnS_4 enhances with increasing post-annealing temperature. However, for thin films annealed at 350 °C, the grain size reduces. Besides, the secondary phase appears in the thin films. These results reveal that the Cu_2ZnSnS_4 phase begins to decompose at 350 °C. The optical band gaps of annealed thin films are 1.48-1.51 eV, which are close to the optimal value for absorber. The experimental results indicate that post-annealing in a sulfur-free atmosphere can further enhance the properties of sulfurized Cu_2ZnSnS_4 thin films. To avoid the decomposition of Cu_2ZnSnS_4 phase, post-annealing should be performed at low temperature. In this work, the optimal post-annealing temperature is 300 °C.

Acknowledgements

This work was funded by National Natural Science Foundation of China (No. 61504029), Doctoral Starting up Foundation of Guangdong University of Technology (No. 15ZK0011) and

Comprehensive Strategic Cooperation Project of Guangdong Province and China Academy of Sciences (No. 2013B091500033).

References

[1] T. Wada, S. Nakamura, T. Maeda, Prog. Photovolt: Res. Appl. **20,** 520 (2012).
[2] A. Redinger, D.M. Berg, P.J. Dale, R. Djemour, L. Gutay, T. Eisenbarth, N. Valle, S. Siebentritt, IEEE J. Photovolt. **1,** 200 (2011).
[3] K. Ramasamy, M.A. Malik, P. O'Brien, Chem. Commun. **48,** 5703 (2012).
[4] S.A. Vanalakar, G.L. Agawane, S.W. Shin, M.P. Suryawanshi, K.V. Gurav, K.S. Jean, P.S. Patil, C.W. Jeong, J.Y. Kim, J.H. Kim, J. Alloys Compd. **619,** 109 (2015).
[5] N.M. Shinde, C.D. Lokhande, J.H. Kim, J.H. Moon, J. Photochem. Photobiol. A **235,** 14 (2012).
[6] X. Jiang, L.X. Shao, J. Zhang, D. Li, W. Xie, C.W. Zou, J.M. Chen, Surf. Coat. Technol. **228,** S408 (2013).
[7] O.K. Simya, A. Mahaboobbatcha, K. Balachander, Superlattices Microstruct. **82,** 248 (2015).
[8] L. Van Puyvelde, J. Lauwaert, P.F. Smet, S. Khelifi, T. Ericson, J.J. Scragg, D. Poelman, R. Van Deun, C. Platzer-Bjorkman, H. Vrielinck, Thin Solid Films **582,** 146 (2014).
[9] J. Ge, J.C. Jiang, P.X. Yang, C. Peng, Z.P. Huang, S.H. Zuo, L.H. Yang, J.H. Chu, Sol. Energy Mater. Sol. Cells **125,** 20 (2014).
[10] W. Wang, M.T. Winkler, O. Gunawan, T. Gokmen, T.K. Todorov, Y. Zhu, D.B. Mitzi, Adv. Energy Mater. **4,** 1301465 (2014).
[11] N. Song, Y. Wang, Y.C. Hu, Y.D. Huang, W. Li, S.J. Huang, X.J. Hao, Appl. Phys. Lett. **104,** 092103 (2014).
[12] F. Aslan, A. Tumbul, J. Alloys Compd. **612,** 1 (2014).
[13] Z. Seboui, A. Gassoumi, N. Kamoun-Turki, Mater. Sci. Semicond. Process. **26,** 360 (2014).
[14] J.X. Xu, Z.M. Cao, Y.Z. Yang, Z.W. Xie, J. Mater. Sci. Mater. Electron. **26,** 726 (2015).
[15] J.X. Xu, Z.M. Cao, Y.Z. Yang, Z.W. Xie, J. Renew. Sustain. Energy **6,** 053110 (2014).
[16] J. Xu, Y. Yang, Z. Xie, Chalcogenide Lett. **11,** 485 (2014).
[17] A. Redinger, D.M. Berg, P.J. Dale, S. Siebentritt, J. Am. Chem. Soc. **133,** 3320 (2011).
[18] J.J. Scragg, T. Ericson, T. Kubart, M. Edoff, C. Platzer-Bjorkman, Chem. Mater. **23,** 4625 (2011).
[19] Y. Ren, J.J. Scragg, T. Ericson, T. Kubart, C. Platzer-Bjorkman, Thin Solid Films **582,** 208 (2015).
[20] A. Khalkar, K.S. Lim, S.M. Yu, S.P. Patole, J.B. Yoo, Electron. Mater. Lett. **10,** 43 (2014).
[21] D. Tiwari, T.K. Chaudhuri, A. Ray, K.D. Tiwari, Thin Solid Films **551,** 42 (2014).
[22] K. Tanaka, M. Kato, H. Uchiki, J. Alloys Compd. **616,** 492 (2014).
[23] G.L. Agawane, A.S. Kamble, S.A. Vanalakar, S.W. Shin, M.G. Gang, J.H. Yun, J. Gwak, A.V. Moholkar, J.H. Kim, Mater. Lett. **158,** 58 (2015).
[24] G.L. Chen, C.C. Yuan, J.W. Liu, Z.G. Huang, S.Y. Chen, W.F. Liu, G.S. Jiang, C.F. Zhu, J. Power Sources **276,** 145 (2015).
[25] U. Chalapathi, S. Uthanna, V. Sundara Raja, J. Renew. Sustain. Energy **5,** 031610 (2013).